Journal of ELECTRONIC MATERIALS, Vol. 45, No. 6, 2016
DOI: 10.1007/s11664-015-4318-z

Preparation and Photoluminescence Properties of $SrAl_2O_4:Eu^{2+},RE^{3+}$ Green Nanophosphors for Display Device Applications

DEVENDER SINGH,[1,2,4] VIJETA TANWAR,[1] ANURA P. SAMANTILLEKE,[2] BERNABE MARI,[3] SHRI BHAGWAN,[1] PRATAP SINGH KADYAN,[1] and ISHWAR SINGH[1]

1.—Department of Chemistry, Maharshi Dayanand University, Rohtak, Haryana 124001, India. 2.—Centro de Fisica, Universidade of Minho, Braga 4710057, Portugal. 3.—Departament de Física Aplicada, Universitat Politècnica de València, Valencia 46022, Spain. 4.—e-mail: devjakhar@gmail.com

An efficient rapid gel combustion process was used to prepare divalent-europium-doped strontium aluminate ($SrAl_2O_4:Eu^{2+}/Eu^{2+},Dy^{3+}/Eu^{2+},Dy^{3+},Nd^{3+}$) nanophosphors in the presence of boron flux in air. The prepared nanophosphors emitted green light at 507 nm upon excitation at 360 nm. The emission of green light was observed due to the $4f^6 5d^1 \rightarrow 4f^7$ transition of Eu^{2+} ions. The absence of the characteristic sharp emission peak at 612 nm for Eu^{3+} ($^5D_0 \rightarrow {}^7F_2$) indicates that efficient reduction of Eu^{3+} to Eu^{2+} occurred in the presence of the boron flux (H_3BO_3) as reducing agent. The x-ray diffraction pattern suggested monoclinic crystallinity, while transmission electron microscopy revealed the average size of the prepared materials to be between 20 nm and 50 nm. Coactivators in the lattices such as Dy^{3+} alone or Dy^{3+} with Nd^{3+} produced long persistence and enhancement of the optoelectronic properties of the prepared materials.

Key words: Rapid gel combustion, green nanophosphors, divalent europium, boron flux, optoelectronic properties

INTRODUCTION

Long-lasting or persistent phosphor materials absorb and trap visible or ultraviolet radiation and then liberate energy to produce visible light, resulting in persistent luminescence.[1,2] Such persistent luminescence of phosphor materials is widely used for various applications, e.g., in dial plates of glow watches, safety indicators, emergency lighting danger signals, automobiles, solar cells, etc.[3–6] Strontium aluminates are such materials, offering outstanding properties such as high quantum efficiency, long afterglow, and excellent chemical stability.[2,7,8] Eu^{2+}-doped MAl_2O_4 (where M can be Sr, Ca, etc.) show good luminescence under ultraviolet (UV) radiation but no persistence. However, doping of Dy^{3+} and Nd^{3+} ions into the $SrAl_2O_4:Eu^{2+}$ lattice improves the persistent luminescence due to the formation of exceedingly dense trapping levels situated at appropriate depth.[9,10] $SrAl_2O_4$ doped with Eu^{2+} and Dy^{3+} finds widespread technological applications as a long-afterglow phosphor.[11,12]

The luminescent characteristics of phosphor materials are often influenced by their method of preparation.[13,14] Conventionally, most long-persistence phosphors consisting of aluminate lattices are synthesized by solid-state reaction in a reductive atmosphere, especially by passing 3% to 5% hydrogen gas with nitrogen gas.[7,8,14–19] These methods are cumbersome, requiring heating at high temperature above 1200°C for about 3 h to 8 h, thereby producing large grain size and poor homogeneity. To obtain smaller grain size, larger grains are milled further, which degrades the optical properties as well as morphology[20] of the material. Several

(Received August 25, 2015; accepted December 19, 2015; published online January 6, 2016)

experimental methods to prepare aluminates phosphors, such as sol–gel processing,[21] sol–gel microwave processing,[22] coprecipitation,[23–25] solvothermal coprecipitation,[26] the reverse microemulsion approach,[27] combustion,[28,29] and microwave combustion,[30,31] have recently been presented.

In continuation of our work on luminescent materials,[15,32,33] the present gel combustion technique was applied for speedy (in minutes) synthesis of $SrAl_2O_4$:Eu^{2+},RE^{3+} nanophosphors in the presence of boron flux as reducing agent in air. The current facile technique is rapid, efficient, energy saving, and low temperature, enabling homogeneous preparation of an aluminate lattice doped with rare-earth ions. Boric acid is used for the boron flux, not only favoring reduction of Eu^{3+} active centers to Eu^{2+} but also improving the crystallinity of the $SrAl_2O_4$:Eu^{2+},RE^{3+} nanophosphors. The crystal structure and surface morphology of the prepared materials were also investigated.

EXPERIMENTAL PROCEDURES

Synthesis of Nanophosphors

Nanosized phosphors were prepared using a rapid gel combustion process.[34,35] Extrapure nitrates $Sr(NO_3)_2$, $Eu(NO_3)_2{\cdot}6H_2O$, $Dy(NO_3)_2{\cdot}6H_2O$, $Nd(NO_3)_2{\cdot}6H_2O$, and $Al(NO_3)_3{\cdot}9H_2O$ as well as N_2H_4CO were weighed according to the stoichiometric compositions $Sr_{0.98}Al_2O_4 : Eu^{2+}_{(0.02)}$, $Sr_{0.96}Al_2O_4 : Eu^{2+}_{(0.02)}$, $Dy^{3+}_{(0.02)}$, and $Sr_{0.95}Al_2O_4 : Eu^{2+}_{(0.02)}, Dy^{3+}_{(0.02)}, Nd^{3+}_{(0.01)}$ in silica crucibles, and boric acid was added at varying ratios with respect to Eu^{3+} ions to optimize the homogeneity and maximum brightness (the suitable ratio of boric acid being found to be 12% of its molecular weight for each 0.01 M Eu^{3+} added).

In each case, all chemicals were mixed in a minimum amount of distilled water with stirring and heating at 80°C for conversion to gel. A calculated amount of urea was then added as fuel for combustion.[34] The mixture in the silica crucible was then put in a preheated muffle furnace set at 500°C. The mixture caught fire immediately (self-ignition), producing a large, voluminous, soft white material. The whole process took about 5 min. The material was taken out and ground to very fine powder. The white powder showed bright green luminescence under UV light, as shown in Fig. 1. The chemical reaction that took place in the combustion of the reactants may be represented as follows:

$$\begin{aligned}&\left[(1-x-y-z)Sr(NO_3)_2\right] + 2\left[Al(NO_3)_3{\cdot}9H_2O\right] \\ &\quad + x\left[Eu(NO_3)_3{\cdot}5H_2O\right] + y\left[Nd(NO_3)_3{\cdot}6H_2O\right] \\ &\quad + z\left[Dy(NO_3)_3.6H_2O\right] + 6N_2H_4CO \rightarrow \\ &\quad Sr_{1-x-y-z}Al_2O_4 : Eu_x, Nd_y, Dy_z \\ &\quad + \text{Gaseous products } [15N_2 + 6CO_2 + 19H_2O].\end{aligned} \tag{1}$$

Instrumentation

Crystal analysis of the phosphor materials was carried out using a Rigaku Ultima IV diffractometer with Cu K_α radiation between 2θ angles of 15° and 70°. Structural study of the compounds was carried out by Fourier-transform infrared (FTIR) spectroscopy using a Nicolet 5700 infrared spectrometer. The oxidation state of the europium dopant (i.e., divalent or trivalent state) in the phosphors was characterized using x-ray photoelectron spectroscopy analysis with an x-ray photoelectron spectroscope (PHI 5000 Versa Prob II). The photoluminescence properties of the phosphor were measured using a SPEX Fluorolog 1680 (USA) fluorimeter equipped with a SPEX 1934 D phosphorimeter with a xenon lamp as excitation source. The morphology of the phosphors was studied using a JEOL JSM-6360LV scanning electron microscope and TECNAI 200 kV (FEI, Electron Optics) transmission electron microscope. Particle sizes were also evaluated from TEM micrographs.

RESULTS AND DISCUSSION

X-ray Diffraction Analysis

The x-ray diffraction (XRD) patterns of the $SrAl_2O_4$:Eu^{2+},RE^{3+} nanophosphors prepared by the rapid gel combustion method are shown in Fig. 2. The phase compositions and crystal size (D) of the materials were evaluated using Scherrer's equation,

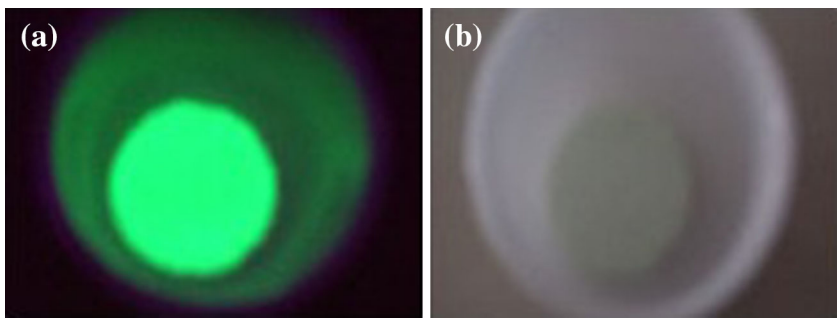

Fig. 1. Typical nanophosphor material (a) under UV excitation (360 nm) and (b) without UV excitation.

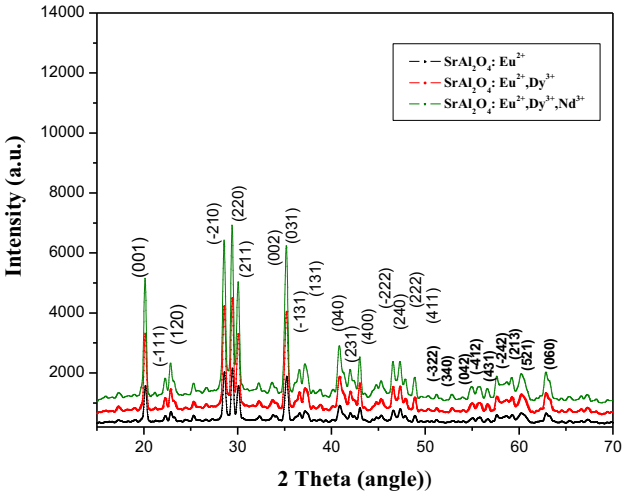

Fig. 2. X-ray diffraction patterns of prepared nanophosphors.

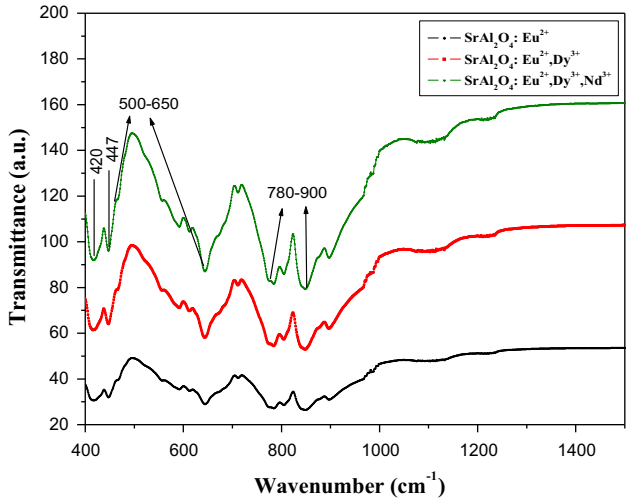

Fig. 3. FTIR spectra of synthesized nanophosphors.

Table I. Calculated particle size for prepared phosphor crystallites

Phosphor material	2θ value	Particle size (nm)
$SrAl_2O_4:Eu^{2+}$	29.42	17.8686
$SrAl_2O_4:Eu^{2+},Dy^{3+}$	29.38	17.8226
$SrAl_2O_4:Eu^{2+},Dy^{3+},Nd^{3+}$	29.44	17.8502

$$D = K\lambda/\beta\cos\theta, \quad (2)$$

where λ is the x-ray wavelength (0.1548 nm) used to obtain the diffraction pattern, K is a constant depending on the grain shape (0.89 to 1.39), θ is the diffraction angle, and β is the full-width at half-maximum (FWHM, in radians) of the most intense peak of the XRD pattern for the material.

The 2θ value and calculated crystallite size are presented in Table I. This analysis showed that the $SrAl_2O_4$ lattice with filled tridymite-like structure exhibits monoclinic lattice structure in space group P_{21}.[36] Strontium ions are situated in the cavities of the interconnected network of aluminate tetrahedra. Two Al^{3+} share one oxygen, as each tetrahedron has one net negative charge. The charge equilibrium is compensated by Sr^{2+} ions residing at interstitial sites within the tetrahedral structure. Because the sizes of Eu^{2+} (1.20 Å) and Sr^{2+} (1.21 Å) are nearly identical, Eu^{2+} ions easily substitute for Sr^{2+}, with no significant distortion being observed in the lattice parameter.[37] The XRD patterns of all the prepared phosphors almost matched with Joint Committee on Powder Diffraction Standards (JCPDS) card no. 34-0379, confirming the formation of the monoclinic crystalline phase of these materials. The codoping with rare-earth ions also did not change the lattice parameters of the $SrAl_2O_4$ matrix, as they are present at concentrations $<0.5\%$ of the whole lattice.

Fourier-Transform Infrared Spectroscopy

The Fourier-transform infrared (FTIR) spectra of the phosphor materials prepared using the rapid gel combustion technique are presented in Fig. 3. In $SrAl_2O_4$, the network is constructed by aluminate tetrahedra with interstitial spaces occupied by Sr^{2+}.[37] The symmetric bending vibration peaks of O–Al–O appeared as a doublet at 450 cm^{-1} and 422 cm^{-1} for all the phosphors. Antisymmetric stretching and antisymmetric bending vibrations appeared at 780 cm^{-1} to 900 cm^{-1} and 500 cm^{-1} to 650 cm^{-1}, respectively, as quartets in the spectra. Addition of higher amounts of boric acid (>30%) results in more broadband signal due to B–O stretching,[38] not being seen in the spectra for our prepared materials, as 12 mol.% boric acid was added in this work.

X-ray Photoelectron Spectroscopy (XPS)

The chemical composition and oxidation states of the various elements (mainly europium) in the $SrAl_2O_4$ phosphors were analyzed using x-ray photoelectron spectroscopy, as shown in Fig. 4. Eu was observed in the spectra at the expected position. The XPS spectra obtained for the Eu^{2+}-doped $SrAl_2O_4$ phosphor established the presence of europium in divalent oxidation state, with two peaks centered at 1126 eV and 1153.4 eV, being assigned to Eu^{2+} $3d_{5/2}$ and $3d_{3/2}$, respectively; if europium were present in trivalent state, then the $3d_{5/2}$ and $3d_{3/2}$ peaks would be found near 1134 eV and 1165 eV, respectively.[39,40] The O 1*s* signal showed an intense peak positioned at 531.5 eV. The Al 2*s* and Al 2*p* signals were located at 133.3 eV and 89.1 eV, respectively. Peaks for Sr 3*s*, Sr 3*p*, and Sr 3*d* were found at 357.2 eV, 287.2 eV, and 135.6 eV, respectively. All peaks of these elements are consistent with standard corresponding central values.

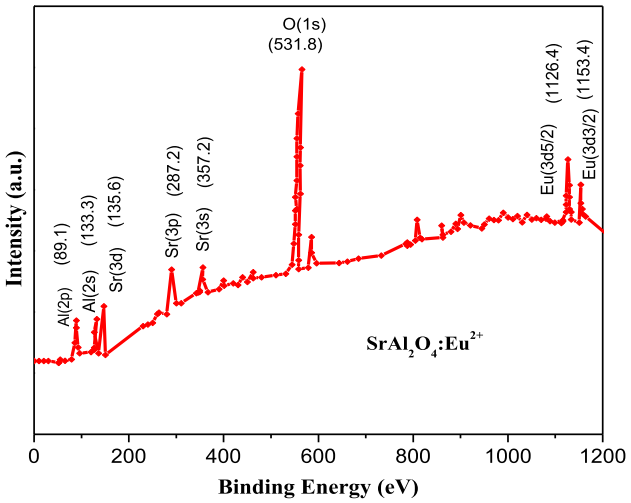

Fig. 4. XPS spectra of $SrAl_2O_4:Eu^{2+}$ phosphor.

Photoluminescence Properties

Figure 5 shows the photoluminescence (PL) spectra of the synthesized $SrAl_2O_4:Eu^{2+},Dy^{3+},Nd^{3+}$ phosphor. It undergoes excitation between 290 nm and 450 nm with a wide band exhibiting a maximum at 360 nm. This wide band corresponds to the transition of the divalent europium ion. The luminescence spectrum of $SrAl_2O_4:Eu^{2+}$ phosphors includes a wide band attributable to the $4f^6 5d^1 \rightarrow 4f^7$ transition of Eu^{2+} ions, emitting green light. This green emission at 507 nm can simply be ascribed to the Eu^{2+} transition, while the complete absence of a sharp emission peak at 612 nm, a characteristic feature of Eu^{3+} emission due to the $^5D_0 \rightarrow {}^7F_2$ transition, indicates the absence of Eu^{3+} ions.

The emission spectrum of a phosphor is affected by the crystal field strength as well as by the degree of covalence of the ions with neighboring oxygen ions. The crystal field strength splits the $5d$ level of the luminescent ion into sublevels, and the luminescence always takes place from the lowest sublevels of the active center. In the $SrAl_2O_4$ lattice, the tetrahedral $[AlO_4]^{5-}$ anion groups form a three-dimensional hard glass network structure, which can effectively protect the Eu^{2+} ions from oxygen in air.[41] Our observation is that the reduction of Eu^{3+} can be controlled by maintaining a proper ratio of boron flux (H_3BO_3). Boric acid is regarded as an outstanding flux to facilitate diffusion of active centers into the host lattice of the material. Hence, it is usually added during preparation of Eu-doped $SrAl_2O_4$ material to lower the forming temperature. Furthermore, the flux forces the dopant and codopant ions to replace Sr^{2+} in the lattice. This increases the dopant and codopant ion concentrations in the aluminate lattice of the material, which helps to sharply increase the luminescence properties of the material. Furthermore, the dissolved B^{3+} ions substitute Al^{3+} ions at their tetrahedral

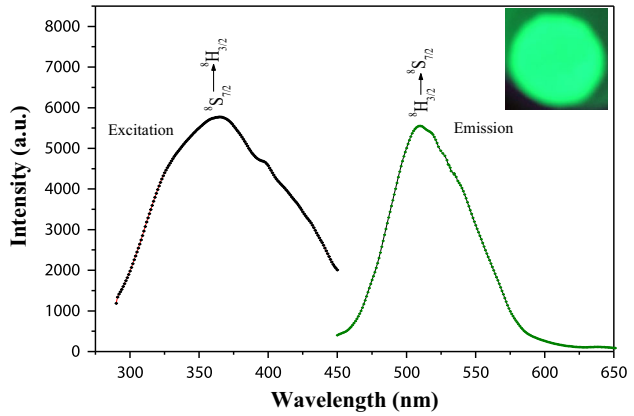

Fig. 5. Excitation and emission spectra of $SrAl_2O_4:Eu^{2+},Dy^{3+},Nd^{3+}$ phosphor.

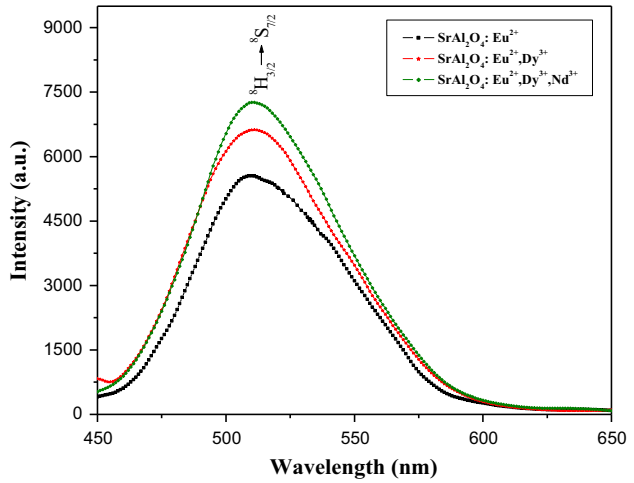

Fig. 6. Emission spectra of prepared nanophosphor materials.

positions, resulting in shrinkage of the host lattice and improvement of the hole-trapping ability of the RE^{3+} ions, which results in enhancement of the luminescence intensity as well as afterglow intensity of the material at low concentration.[42,43] Pei et al.[43] and Machida et al.[44] suggested that the anionic $[BO_4]^{5-}$ tetrahedra most probably formed during the reaction are believed to play an effective role in electron transfer during the process of reduction of Eu^{3+} to Eu^{2+}. Chen et al. also showed that the luminescence intensity as well as afterglow lifetime were considerably enhanced with B_2O_3 addition in $SrAl_2O_4:Eu^{2+}$ phosphor.[37,38]

On introduction of different codopants, i.e., Dy^{3+} alone or in combination with Nd^{3+}, into the $SrAl_2O_4:Eu^{2+}$ phosphor lattice, we observed enhancement in the photoluminescence intensity, as shown in Fig. 6. Addition of codopants induces formation of hole traps (between the excited state and ground state of Eu^{2+}). A higher concentration of codopants results in more hole-trap levels, leading to an enhancement of the photoluminescence properties

of the material.[9,16] The maximum brightness was achieved when incorporating both Dy^{3+} and Nd^{3+} codopants into the host lattice.

The Commission Internationale de l'Eclairage (CIE) color coordinates of the prepared nanophosphors are presented in Fig. 7 and Table II. For all the prepared samples, the CIE color coordinates fall in the bright green region.

Afterglow Properties of the Nanophosphors

The long-afterglow performance of these materials is demonstrated in Fig. 8. The samples were excited with UV light (365 nm) for 10 min, and the decay profiles were obtained for different codopants in the $SrAl_2O_4$ lattice. Several authors have measured the afterglow of $SrAl_2O_4$:Eu^{2+},Dy^{3+} phosphor using different orders of exponential decay curve.[1,3,7,42] We analyzed the afterglow decay of the prepared phosphor materials using the exponential equation[45,46]

$$I = I_0 + A_1 \exp(-t/\tau_1) + A_2 \exp(-t/\tau_2), \qquad (3)$$

where I is the phosphorescence intensity at any time t after cutting off the UV excitation, I_0, A_1, and A_2 are constants, and τ_1 and τ_2 are the decay times for the exponential components of the studied material.

The decay parameters for the phosphors are presented in Table III. The above equation suggests that there are two types of trapping levels available in the lattice of the material, having different values τ_1 and τ_2, which reflect the concentrations of shallow and deeper trap levels in the lattice of the phosphors. Longer decay times can be due to deeper trap levels, while higher initial intensity is due to the density of shallow trap levels.[15,16] The average decay lifetime was also calculated from the following equation[47]:

$$\tau_{ave} = \left(A_1\tau_1^2 + A_2\tau_2^2\right)/(A_1\tau_1 + A_2\tau_2). \qquad (4)$$

The emission lifetime of a phosphor is influenced by the depth and type of the trap levels. The long-afterglow persistence of the phosphors is due to Eu^{2+}, which acts as a luminescent center, and Dy^{3+}/Dy^{3+}+Nd^{3+}, which result in trap levels in the lattice. On removal of the excitation source from the material, trapped holes move thermally to the valence band and then recombine with excess electrons at metastable-state sites, leading to persistent luminescence in these materials.[8] The luminescence decay characteristics of the codoped phosphors investigated at 507 nm emission indicate that the materials emit light far longer than the

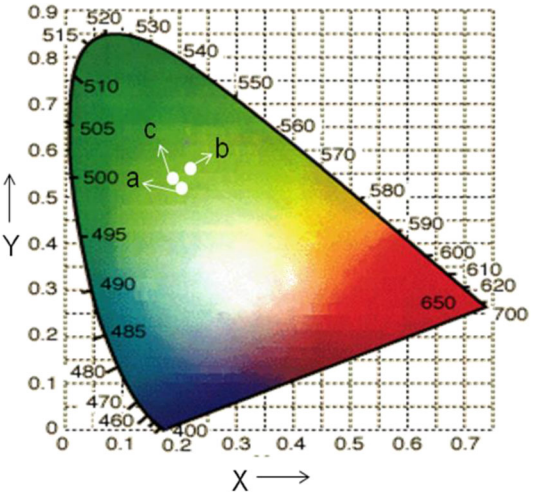

Fig. 7. Chromaticity diagram of (a) $SrAl_2O_4$:Eu^{2+}, (b) $SrAl_2O_4$:Eu^{2+},Dy^{3+}, and (c) $SrAl_2O_4$:Eu^{2+},Dy^{3+},Nd^{3+} synthesized nanophosphors.

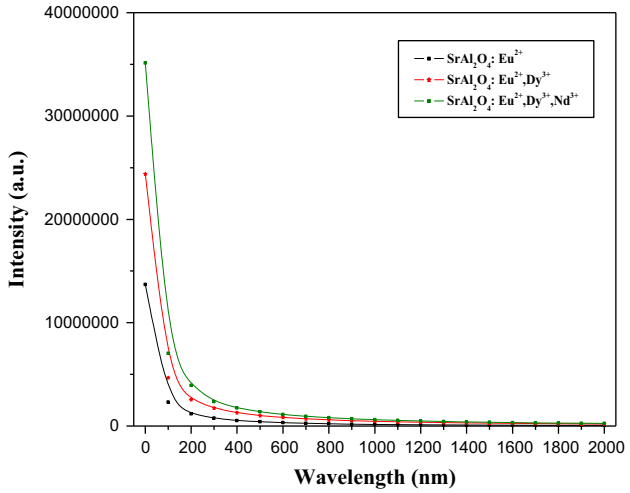

Fig. 8. Decay curves of prepared nanophosphor materials.

Table II. CIE color coordinates of synthesized nanophosphors

	Phosphor compound	Coordinates	
		x	*y*
a	$SrAl_2O_4$:Eu^{2+}	0.1924	0.5051
b	$SrAl_2O_4$:Eu^{2+},Dy^{3+}	0.1972	0.5688
c	$SrAl_2O_4$:Eu^{2+},Dy^{3+},Nd^{3+}	0.1845	0.5422

Table III. Parameters from second-order exponential decay fitting for prepared nanomaterials

	Decay parameters					
Nanophosphor	I_o	A_1	τ_1 (s)	A_2	τ_2 (s)	τ_{ave} (s)
$SrAl_2O_4:Eu^{2+}$	0.00321	0.7134	34.40525	4.871	48.69098	47.35122345
$SrAl_2O_4:Eu^{2+},Dy^{3+}$	0.07141	0.5741	34.14092	8.423	58.41938	57.48935052
$SrAl_2O_4:Eu^{2+},Dy^{3+},Nd^{3+}$	0.07361	0.5534	67.90022	8.514	73.14384	72.84544925

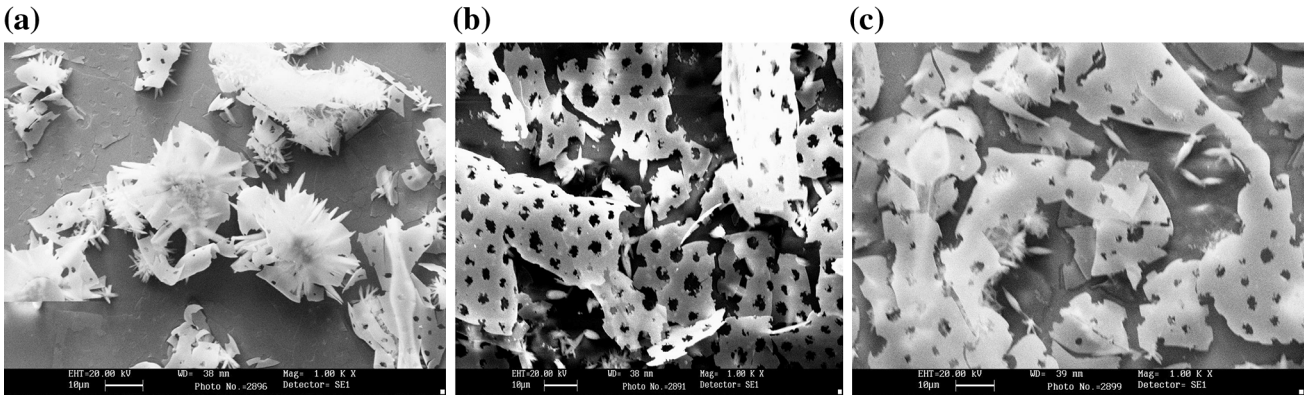

Fig. 9. SEM morphology of (a) $SrAl_2O_4:Eu^{2+}$, (b) $SrAl_2O_4:Eu^{2+},Dy^{3+}$, and (c) $SrAl_2O_4:Eu^{2+},Dy^{3+},Nd^{3+}$ nanophosphors.

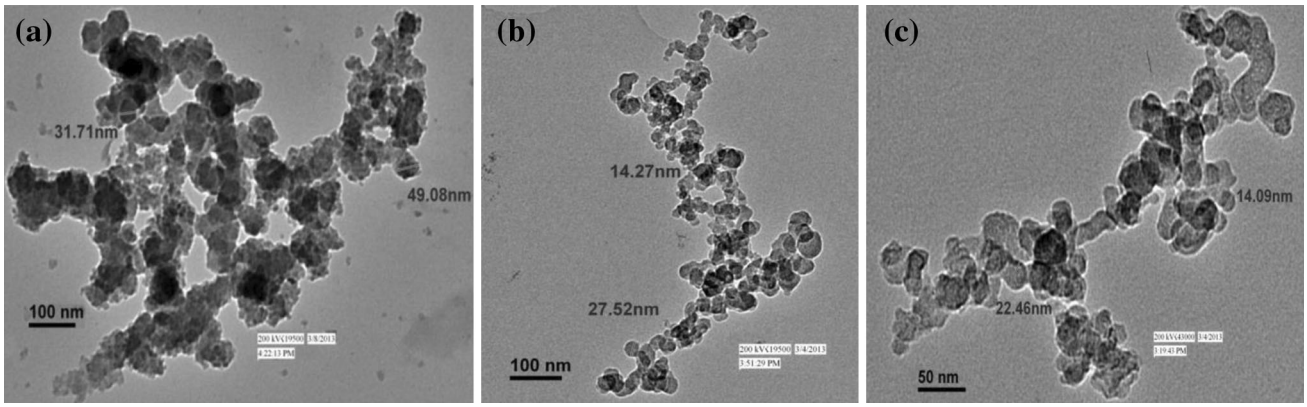

Fig. 10. TEM micrographs of (a) $SrAl_2O_4:Eu^{2+}$, (b) $SrAl_2O_4:Eu^{2+},Dy^{3+}$, and (c) $SrAl_2O_4:Eu^{2+},Dy^{3+},Nd^{3+}$ nanophosphors.

lifetime of Eu^{2+}.[15,16,48] This indicates the presence of persistent luminescence in these materials. The decay characteristics showed no significant changes with different irradiation times.

Morphological Investigation

Scanning Electron Microscopy (SEM)

To determine the morphology of the materials, scanning electron micrographs were taken as shown in Fig. 9, which indicate complete combustion of the material resulting in very fluffy powder. The surfaces show cracks, voids, and flakes formed by the huge amount of escaping gases. The reason for the vacant spaces may be redox reaction between fuel and metal nitrates, due to which a large amount of combustible gases are produced, as shown by the chemical reaction in Eq. 1. The escaping gases thereby avoid sintering of the material, prevent agglomerations, and help to disintegrate the material into the nanocrystalline phase. The huge amount of gaseous products is released as a result of the violent combustion, causing pore formation and resulting in fluffy phosphor material.

Tunneling Electron Microscopy (TEM)

The particle sizes of the synthesized phosphors were analyzed from transmission electron micrographs.

TEM analysis enabled detailed microstructural analysis of the phosphor particles. Figure 10 shows TEM micrographs of the phosphors synthesized using the presented combustion method at 500°C. The particle size of these phosphors as estimated by TEM was found to be in good agreement with the size estimated using Scherrer's equation, lying in the nanosize range.

CONCLUSIONS

Nanosized green $SrAl_2O_4:Eu^{2+}$, $SrAl_2O_4:Eu^{2+}$, Dy^{3+}, and $SrAl_2O_4:Eu^{2+},Dy^{3+},Nd^{3+}$ nanophosphors were efficiently prepared in the presence of boron flux using a rapid gel combustion technique. The boron flux (H_3BO_3) promoted entry of activator ions into the crystal lattice, helping formation of luminescent centers, and also improved the crystallinity as well as facilitating reduction of Eu^{3+} to Eu^{2+}. Under ultraviolet excitation, the synthesized phosphors exhibited bright green emission at 507 nm associated with the $4f^6(^7F_J)5d^1(t_2g) \rightarrow 4f^7(^8S_{7/2})$ transition of Eu^{2+} ions present in the aluminate lattice. XRD analysis of the crystallites showed monoclinic crystalline phase. SEM and TEM techniques also confirmed the formation of nanosized crystallites of the prepared phosphors. The nanophosphors prepared by the presented rapid gel combustion technique exhibited high brightness and long afterglow, potentially making them suitable for use in various optoelectronic display device applications.

ACKNOWLEDGEMENTS

The authors gratefully recognize the financial support from the University Grant Commission (UGC), New Delhi [MRP-40-73/2011(SR)] and European Commission through Nano CIS Project (FP7-PEOPLE-2010-IRSES ref. 269279).

REFERENCES

1. C. Chang, L. Jiang, D. Mao, and C. Feng, *Ceram. Int.* 30, 285 (2004).
2. C. Chang, D. Mao, J. Shen, and C. Feng, *J. Alloys Compd.* 348, 224 (2003).
3. T. Katsumata, T. Nabae, K. Sasajima, S. Kumuro, and T. Morikawa, *J. Electrochem. Soc.* 144, L243 (1997).
4. Y. Murayama, N. Takeuchi, Y. Aoki, and T. Matsuzawa, US Patent No. 5 424 (1995) 006.
5. P.D. Sarkisov, N.V. Popovich, and A.G. Zhelnin, *Glass Ceram.* 60, 309 (2003).
6. S.K. Yesilay, B. Karasu, G. Kaya, and E. Karacaoglu, *Adv. Sci. Technol.* 62, 88 (2010).
7. A. Nag and T.R.N. Kutty, *J. Alloys Compd.* 354, 221 (2003).
8. T. Matsuzawa, Y. Aoki, N. Takeuchi, and Y. Murayama, *J. Electrochem. Soc.* 143, 2670 (1996).
9. K.V.D. Eeckhout, P.F. Smet, and D. Poelman, *Materials* 3, 2536 (2010).
10. M. Lastusaari, H.F. Brito, S. Carlson, J. Hölsä, T. Laamanen, L.C.V. Rodrigues, and E. Welter, *Phys. Scr.* **89**, Article ID 044004 (2014).
11. J. Botterman, J.J. Joos, and P.F. Smet, *Phys. Rev. B* **90**, Article ID 085147 (2014).
12. D. Jia, *Opt. Mater.* 22, 65 (2003).
13. C.H. Lu, W.T. Hsu, C.H. Huang, S.V. Godbole, and B.M. Cheng, *Mater. Chem. Phys.* 90, 62 (2005).
14. Y.H. Lin, Z.T. Zhang, F. Zhang, Z.L. Tang, and Q.M. Chen, *Mater. Chem. Phys.* 65, 103 (2000).
15. S.D. Han, K.C. Singh, T.Y. Cho, H.S. Lee, D. Jakhar, J.P. Hulme, C.H. Han, J.D. Kim, I.S. Chun, and J. Gwak, *J. Lumin.* 128, 301 (2008).
16. W. Jia, H. Yuan, L. Lu, H. Liu, and W.M. Yen, *J. Lumin.* 76–77, 424 (1998).
17. S.Y. Kaya, E. Karacaoglu, and B. Karasu, *Ceram. Int.* 38, 3701 (2012).
18. I.C. Chen and T.M. Chen, *J. Mater. Res.* 16, 644 (2001).
19. J. Holsa, H. Jungner, M. Lastusaari, and J. Niittykoski, *J. Alloys Compd.* 323–324, 326 (2001).
20. L. Xiao, S. Meng, Z. Junying, and W. Tianmin, *J. Rare Earths* 28, 150 (2010).
21. T.Y. Peng, H.J. Liu, H.P. Yang, and C.H. Yan, *Mater. Chem. Phys.* 85, 68 (2004).
22. W. Suli, Z. Shufen, and Y. Jinzong, *Mater. Chem. Phys.* 102, 80 (2007).
23. C.K. Chang, Z.X. Yuan, and D.L. Mao, *J. Alloys Compd.* 415, 220 (2006).
24. S.V. Gabelkov, R.V. Tarasov, N.S. Poltavtsev, Y.P. Kurilo, M.P. Starolat, N.F. Andrievskaya, A.G. Mironova, E.G. Ledovskaya, L.M. Litvinenko, and F.V. Belkin, *Inorg. Mater.* 43, 398 (2007).
25. J.S. Kim, *J. Ceram. Process. Res.* 10, 443 (2009).
26. X.U.E. Zhiping, D.E.N.G. Suqing, L.I.U. Yingliang, L.E.I. Bingfu, X.I.A.O. Yong, and Z.H.E.N.G. Mingtao, *J. Rare Earths* 31, 241 (2013).
27. C.H. Lu, S.Y. Chen, and C.H. Hsu, *Mater. Sci. Eng. B* 140, 218 (2007).
28. T.Y. Peng, H.P. Yang, X.L. Pu, B. Hu, Z.C. Jiang, and C.H. Yan, *Mater. Lett.* 58, 352 (2004).
29. Z.L. Fu, S.H. Zhou, Y.N. Yu, and S.Y. Zhang, *Chem. Phys. Lett.* 395, 285 (2004).
30. D.S. Kshatri, A. Khare, and P. Jha, *Chalcogenide Lett.* 10, 121 (2013).
31. T.T. Lai, C.C. Chang, C.Y. Yang, S. Das, and C.H. Lu, *Ceram. Int.* 39, 159 (2013).
32. D. Singh, V. Tanwar, S. Bhagwan, A.P. Simantilleke, I. Singh, and P.S. Kadyan, *Adv. Sci. Lett.* 20, 1531 (2014).
33. S.D. Han, C.H. Han, I. Singh, and D. Singh, *Ind. J. Chem.* 43A, 2542 (2004).
34. S. Ekambaram, K.C. Patil, and M. Maaza, *J. Alloys Compd.* 393, 81 (2005).
35. F. Clabau, X. Rocquefelte, S. Jobic, P. Deniard, M.H. Whangbo, A. Garcia, and T. Le Mercier, *Chem. Mater.* 17, 3904 (2005).
36. D. Haranath, V. Shanker, H. Chander, and P. Sharma, *J. Phys. D Appl. Phys.* 36, 2244 (2003).
37. I.C. Chen and T.M. Chen, *J. Mater. Res.* 16, 1293 (2001).
38. J. Chen, F. Gu, and C. Li, *Cryst. Growth Des.* 8, 3175 (2008).
39. W.B. Im, J.H. Kang, D.C. Lee, S. Lee, D.Y. Jeon, Y.C. Kang, and K.Y. Jung, *Solid State Commun.* 133, 197 (2005).
40. J. Zhang, M. Yang, H. Jin, X. Wang, X. Zhao, X. Liu, and L. Peng, *Mater. Res. Bull.* 47, 247 (2012).
41. C. Zhu, Y. Yang, X. Liang, S. Yuan, and G. Chen, *J. Am. Ceram. Soc.* 90, 2984 (2007).
42. J. Niittykoski, T. Aitasalo, J. Holsa, H. Jungner, M. Lastusaari, M. Parkkinen, and M. Tukia, *J. Alloys Compd.* 374, 108 (2004).
43. Z. Pei, Q. Zeng, and Q. Su, *J. Phys. Chem. Solids* 61, 9 (2000).
44. K. Machida, G. Adachi, and J. Shiokawa, *J. Lumin.* 21, 101 (1979).
45. R. Pang, C. Li, L. Shi, and Q. Su, *J. Phys. Chem. Solids* 70, 303 (2009).
46. C.H. Huang and T.M. Chen, *Opt. Express* 18, 5089 (2010).
47. G. Lee, W.B. Im, A. Kirakosyan, S.H. Cheong, J.Y. Han, and D.Y. Jeon, *Opt. Express* 21, 3287 (2013).
48. D.S. Kshatri, A. Khare, and P. Jha, *Optik* 124, 2974 (2013).